Structural peculiarities of cementite and their influence on magnetic characteristics

2007 J. Phys.: Condens. Matter 19 196214

(http://iopscience.iop.org/0953-8984/19/19/196214)

IOP PUBLISHING JOURNAL OF PHYSICS: CONDENSED MATTER

J. Phys.: Condens. Matter **19** (2007) 196214 (9pp) doi:10.1088/0953-8984/19/19/196214

Structural peculiarities of cementite and their influence on magnetic characteristics

A K Arzhnikov[1], L V Dobysheva[1] and C Demangeat[2]

[1] Physical–Technical Institute, Ural Branch of Russian Academy of Sciences, Kirov Street 132, Izhevsk 426001, Russia
[2] Institut de Physique et Chimie des Matériaux de Strasbourg, (UMR CNRS-ULP 7504), 23, rue du Loess, 67034 Strasbourg, France

E-mail: arzhnikov@otf.pti.udm.ru

Received 18 January 2007, in final form 27 February 2007
Published 19 April 2007
Online at stacks.iop.org/JPhysCM/19/196214

Abstract

The iron carbide Fe_3C has been studied by first-principles density-functional theory. Both prismatic and octahedral environments of the carbon atoms have been considered. The crystal structure with the carbon position in a prismatic environment possesses the lowest total energy. The energy of the magneto-crystalline anisotropy is an order of magnitude higher in the prismatic modification than in the octahedral one. The room-temperature behaviour of the coercive force on the temperature of annealing of plastically deformed samples has been explained by this fact. A difference in Mössbauer parameters (electric field gradient (EFG), and the angles between the EFG and the hyperfine field) found for the two positions of carbon in the cementite lattice looks promising for experimental detection of the presence of carbon with octahedral environment in plastically deformed samples.

1. Introduction

The study of the properties of cementite, i.e. iron carbide Fe_3C, has been conducted for a long time. Originally, cementite was investigated in order to improve the mechanical properties of steels. The magnetic properties have also received some attention in connection with nondestructive methods of the control of steel.

More precisely, the recent interest in the properties of Fe_3C may be explained by new possibilities of obtaining metastable compounds by mechanical alloying, implantation and so forth (see, for example, [1–4]). Besides, the monophase Fe_3C itself has attracted considerable interest due to peculiarities in the bulk-modulus behaviour [5] and the instability of the magnetic state under pressure [6, 7]. Finally, an additional impact has been given by the studies dealing with the chemical composition of the Earth's core [8, 9].

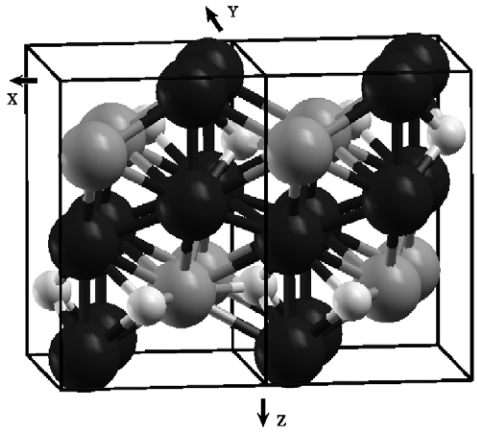

Figure 1. Double unit cell of cementite with prismatic environment of the carbon atoms. Large grey and black balls show iron Fe1 (S position) and Fe2 (G position) atoms; small white balls represent carbon.

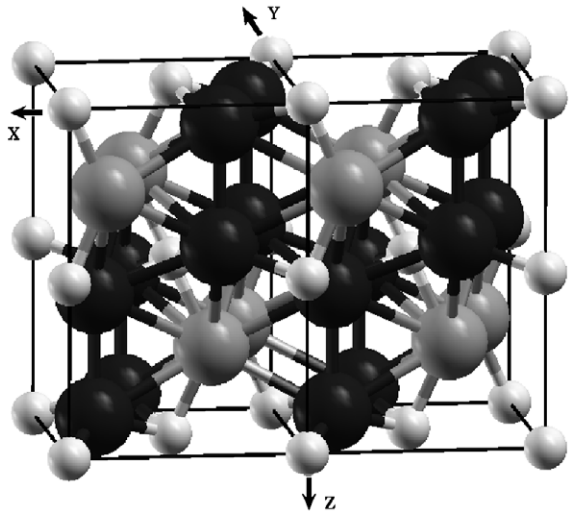

Figure 2. Double unit cell of cementite with octahedral environment of the carbon atoms. Large grey and black balls show iron Fe1 (S position) and Fe2 (G position) atoms; small white balls represent carbon.

The arrangement of iron atoms in the cementite structure was detected by x-ray diffraction [10] but the carbon location in the lattice does not appear to be absolutely clear. Even in the very thorough experiments of [10] the authors made a number of simplifications during the x-ray data processing (see a critical review of this and other papers in [11]). According to [12] the carbon atoms can occupy four positions between the iron sites. Two of them (prismatic and octahedral, figures 1 and 2) are often specified as possible places for the carbon atoms. The two other places named by authors of [12] as distorted prismatic and octahedral positions have not been discussed before. Since the carbon in these two last positions is very close to iron atoms (0.16 and 0.12 nm against 0.19 nm in undistorted positions), these modifications appear to be improbable and we do not consider them here. The experiments

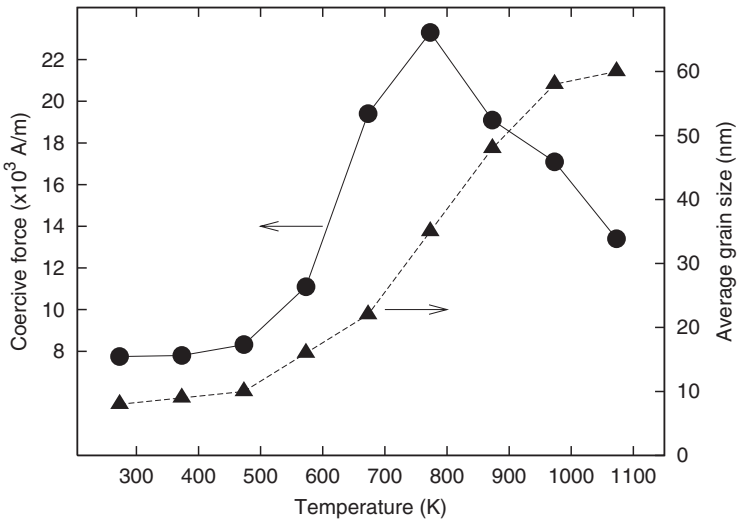

Figure 3. The coercive force (●) and average grain size (▲) of cementite prepared by plastic deformation as a function of annealing temperature taken from experiments performed at room temperature in [14].

made on specially prepared samples annealed at high temperature are related to the ground state of cementite. The powder neutron diffraction on such samples in [13] shows only the prismatic position of carbon. Concerning the non-equilibrium samples, the present-day experimental data on cementite testify only that the carbon positions actually depend critically on the mechanical and thermal treatment. The relevant structural changes manifest themselves in both the mechanical and magnetic properties. Figure 3, drawn from the experimental data obtained in [14], shows the coercive force at room temperature of cementite prepared by plastic deformation, as a function of the annealing temperature. Such an increase of the coercive force with grain size was observed and easily explained in soft-magnetic materials where the domain-wall width is a few times larger than the characteristic grain size [15]. For the samples under study, the domain-wall width is smaller than the grain size (see below), so the behaviour of the coercive force remains clearly uncommon.

We strongly believe that this uncommon behaviour should be linked to the redistribution of the carbon atoms in the Fe_3C lattice: without such a redistribution, annealing would decrease the coercive force because of the growth of the grains (figure 3) and disappearance of the imperfections. Besides, one can find other experimental evidence of the different carbon atom positions in different samples like the change in the nearest environment before and after annealing obtained in EELFS (electron energy loss fine structure) [16], changes in the Mössbauer spectra with annealing [17] and so forth.

This paper studies, through first-principles calculations, the possibility of different positions of carbon in Fe_3C and the effect on physical properties. Previous theoretical investigations of cementite have been carried out (see, for example, [6, 9, 18, 19]), but only in [18] was an attempt made to obtain some characteristics of cementite with prismatic or octahedral positions of the carbon atoms. Thus, the main purpose of the present paper is to calculate, taking into account lattice relaxations, and compare the total energy, magneto-crystalline energy, magnetic moments and the parameters of hyperfine interaction of cementite with different positions of carbon atoms.

2. Models and methods of calculation

The crystal structure of Fe_3C is an orthorhombic lattice: we use the $Pbnm$ space group. The unit cell contains 12 iron atoms and 4 carbon atoms (a double unit cell, drawn with the help of the package [20] in figures 1 and 2, represents respectively the prismatic and octahedral modifications). In these figures, four iron atoms occupy the special S position and are marked Fe1 whereas the remaining eight iron atoms of Fe2 type are at the general G position. The nearest neighbours of Fe1 are carbon atoms, and the next-nearest-neighbouring shell of an Fe1 atom consists of 12 iron atoms at slightly different distances. The nearest neighbours of Fe2 are also carbon atoms, and the next-nearest-neighbouring shell of an Fe2 atom contains 11 iron atoms.

The calculations presented in this paper were conducted by the full-potential linearized augmented plane wave (FLAPW) method in the WIEN2k package [21]. The generalized gradient approximation of the exchange–correlation potential (GGA) [22] was used in this work. In the FLAPW method the wave functions, charge density and potential are expanded in spherical harmonics within non-overlapping muffin-tin (MT) spheres of radius R_{MT} and in plane waves in the remaining space of the unit cell (interstitial region). The basis set is split into core and valence parts. The core states are treated with the spherical part of the potential and are assumed to have a spherically symmetric charge density totally confined inside the muffin-tin spheres; they are treated in a fully relativistic way. The expansion of the valence wave functions inside the MT spheres is confined to $l_{max} = 10$ and they are treated within a potential expanded into spherical harmonics up to $l = 4$. We used a mixed LAPW (Fe-sp states)/APW + lo (local orbital) [23] (Fe-d states) basis set. The wave functions in the interstitial region were expanded in plane waves with a cutoff K_{max} determined by the relation $R_{MT}K_{max} = 7$. The charge density was Fourier expanded up to $G_{max} = 20$. The relaxation of the size of the unit cell and of the atomic positions was conducted in the scalar-relativistic approximation for the valence electron, with a mesh of 60 special k-points in the irreducible wedge of the Brillouin zone. All the parameters used were chosen in a standard for the WIEN2k package way. The energy of the magneto-crystalline anisotropy E_{MA} was calculated including the spin–orbit coupling through the second variational method [21]. Its calculation, unlike other properties studied, requires special attention because the accuracy of the total energies must be as good as 1×10^{-5} Ryd. Thus, after the usual convergence without account of the spin–orbit interaction (SOI), the number of k-points was enlarged and the iterative procedure with SOI was performed with the criterion of charge convergence of $1–2 \times 10^{-6}$ (this is a mean-squared distance between the input and output electron density in the iteration scheme). The convergence of E_{MA} on the number of k-points (280, 432 and 630 k-points in the irreducible wedge of the Brillouin zone), K_{max} ($7/R_{MT}$ and $7.5/R_{MT}$) and the upper boundary of the electron states taken into account in SOI (0.65 and 2.15 Ryd above the Fermi energy) was checked. The variation of E_{MA} with the changes of parameters was 1×10^{-5} Ryd.

3. Results and discussion

As pointed out before, we have calculated two different periodical systems. Tables 1 and 2 give data for each system for two sizes of the unit cell. The sizes of the unit cell for the modification with prismatic environment of carbon (figure 1) are $\{a, b, c\} = \{0.4523, 0.5089, 0.6743\}$ nm or $\{0.4481, 0.5056, 0.6743\}$ nm. The first set corresponds to the experimental values obtained by x-ray diffraction for the annealed samples in [14]; they are similar to previous values reported in the literature (see for example [10]). These parameters used in the first calculation are designated as model 1. The second set of lattice parameters (model 2) have been obtained

Table 1. The structural parameters of the unit cell—lattice parameters (nm) and positions (fractional coordinates) of the atoms—obtained in experiments (exp.) [10] and used in calculations (Model 1 and Model 2; see text) for cementite with a prismatic environment of carbon.

	x			*y*			*z*		
	Exp	Model 1	Model 2	Exp	Model 1	Model 2	Exp	Model 1	Model 2
Lat. par.	0.4523	0.4523	0.4490	0.5089	0.5089	0.5047	0.6743	0.6743	0.6743
Fe1	0.8330	0.8367	0.8367	0.0400	0.0361	0.0361	0.2500	0.2500	0.2500
Fe2	0.3330	0.3313	0.3313	0.1750	0.1755	0.1755	0.0650	0.0677	0.0677
C	0.4300[a]	0.4384	0.4384	0.8700[a]	0.8760	0.8760	0.2500[a]	0.2500	0.2500

[a] The position of carbon cannot be well defined in the x-ray diffraction experiments; so, in the literature data, it is mainly assumed from structural considerations.

Table 2. The structural parameters of the unit cell—lattice parameters (nm) and positions (fractional coordinates) of the atoms—obtained in experiments (exp.) [10] and used in calculations (Model 1 and Model 2; see text) for cementite with an octahedral environment of carbon.

	x		*y*		*z*	
	Model 1	Model 2	Model 1	Model 2	Model 1	Model 2
Lat. par.	0.4523	0.4711	0.5089	0.5111	0.6743	0.6960
Fe1	0.8231	0.8342	0.0472	0.0452	0.2500	0.2500
Fe2	0.3479	0.3450	0.1713	0.1705	0.0784	0.0752
C[a]	0.0	0.0	0.0	0.0	0.0	0.0

[a] Usually, in the processing of experimental data, the octahedral position is not considered; so, these values equal those obtained from structural considerations in [11].

in the present work from the total-energy minimization. In both cases (model 1 and model 2) the atoms of the unit cell have been shifted into positions where the resulting forces acting on the atoms are zero. As the experimental and the equilibrium lattice parameters do not differ significantly (the cell-volume change is 1.6%) the fractional coordinates of atoms corresponding to the energy minimum in model 1 are equal to those in model 2, within calculation accuracy.

For the case of octahedral environment of carbon (figure 2), the unit-cell sizes are chosen as $\{a, b, c\} = \{0.4523, 0.5089, 0.6743\}$ nm or $\{0.4711, 0.5111, 0.6960\}$ nm. As there are no experimental data for the octahedral modification, the first set (model 1) equals that of the prismatic one, i.e., corresponds to the experimental data for the well-annealed samples. The second set of unit-cell sizes (model 2) corresponds to the equilibrium unit-cell sizes at which the total-energy minimum is realized. For both models, the atoms have been shifted to the positions with zero resulting forces. Here, the equilibrium unit-cell sizes (model 2) are larger than in model 1 (the cell volume differs by 8%), so the fractional coordinates appear to be slightly different in the two models. Note here that the difference in the lattice parameters between the two modifications can explain the experimental enlargement of the unit cell in plastically deformed cementite in [1], where, as we believe, a mixture of two modifications is realized.

It is well known that the equilibrium values of unit-cell sizes depend on the approximation of the exchange–correlation potential and the calculation scheme. Thus, the magnetic properties can change essentially, even to the point of magnetic-order disappearance as seen, for example, in Cr [24]. In the present work the change of the magnetic properties within the

Table 3. Spin M_{spin} and orbital M_{orb} magnetic moments, Fermi-contact H_{spin} and orbital H_{orb} contributions to the hyperfine magnetic field H, isomer shift IS, electric field gradient V_{zz}, asymmetry parameter η, polar θ and azimuthal ϕ angles of H, and calculated and experimental quadrupole splitting Δ for the prismatic case with experimental sizes of the unit cell (Model 1).

	Fe1	Fe2
M_{spin} (μ_B)	2.01	1.94
M_{orb} (μ_B)	0.05	0.04
H_{spin} (T)	−25.5	−25.0
H_{orb} (T)	3.1	2.7
$H = H_{spin} + H_{orb}$ (T)	−22.4	−22.3
IS (mm s^{-1})	0.181	0.186
V_{zz} ($\times 10^{21}$ V m^{-2})	3.12	1.33
η	0.11	0.62
θ (grad)	90	132.54
ϕ (grad)	90	11.6
Δ (mm s^{-1})	0.49	0.22
Δ_{exp} (mm s^{-1}) [29]	0.58	0.32

Table 4. Spin M_{spin} and orbital M_{orb} magnetic moments, Fermi-contact H_{spin} and orbital H_{orb} contributions to the hyperfine magnetic field H, isomer shift IS, electric field gradient V_{zz}, asymmetry parameter η, polar θ and azimuthal ϕ angles of H, and quadrupole splitting Δ calculated for the prismatic and octahedral cases with equilibrium sizes of unit cell (Model 2).

	Prismatic		Octahedral	
	Fe1	Fe2	Fe1	Fe2
M_{spin} (μ_B)	1.97	1.91	2.09	1.90
M_{orb} (μ_B)	0.05	0.04	0.05	0.03
H_{spin} (T)	−25.1	−24.7	−24.3	−23.7
H_{orb} (T)	3.1	2.7	3.1	1.9
$H = H_{spin} + H_{orb}$ (T)	−22.0	−22.0	−21.2	−21.8
IS (mm s^{-1})	0.162	0.169	0.221	0.139
V_{zz} ($\times 10^{21}$ V m^{-2})	3.07	1.37	1.99	−2.09
η	0.05	0.83	0.996	0.23
θ (grad)	90	138.58	90	73.12
ϕ (grad)	0	11.17	90	26.6
Δ (mm s^{-1})	0.48	0.24	0.36	0.33

studied range of sizes remains small (2% for the Fe magnetic moments) and does not drastically affect the conclusions. Nevertheless, we have found it suitable to specify the results of the calculations for all the unit-cell sizes under study (see tables 3 and 4).

The difference in energy between the two cases with different carbon positions is $E_{oct} - E_{pris} \approx 0.0075$ Ryd/at at experimental sizes of the unit cell (model 1) and $E_{oct} - E_{pris} \approx 0.0050$ Ryd/at at equilibrium sizes of the unit cell (model 2). This confirms clearly that the modification with the prismatic carbon position is the ground state, in full agreement with experimental results.

The energy difference obtained is smaller than the energy inserted during plastic deformation in mechanical alloying ($E_{deform} \approx 7$–14×10^5 J kg^{-1} $= 6$–12×10^{-3} Ryd/at [25]). This allows us to assert that plastic deformation can transform the prismatic environment of

carbon into a metastable state with octahedral environment. On the other hand, the energy difference $E_{\mathrm{oct}} - E_{\mathrm{pris}}$ corresponds to a small probability of the nucleation of the metastable phase at the annealing temperature $T < 700$ K. So, at such an annealing temperature, only a transition from metastable states to the ground one (with prismatic environment of carbon) may occur, and not the other way round.

The dependence of the magneto-crystalline energy E_{MA} on the carbon position is of utmost interest for us. Before presenting our results, let us remember that for transition metals E_{MA} it is generally difficult to determine because it is generally a small value resulting from the difference of two large quantities and it is quite close to the level of numerical accuracy. Fortunately, here, E_{MA} for the case with the prismatic environment of carbon is very much larger than that determined for the octahedral case, so we are pretty convinced that the results are reliable. The calculations show that the [001] direction is an easy magnetization axis and the [010] one is a hard magnetization axis. E_{MA} (i.e. the difference in total energy between the states with magnetization along these two axes per volume), in the prismatic case, is given by

$$E_{\mathrm{MA}} = E_{[010]} - E_{[001]} = 7 \times 10^{-5}\ \mathrm{Ryd/cell} = 9.8 \times 10^{5}\ \mathrm{J\,m^{-3}}.$$

E_{MA} at experimental and equilibrium unit-cell size does not differ within calculation accuracy, as the cell sizes differ little in the two models. The easy-magnetization axis and the magnitude of E_{MA} correspond to those obtained in the experiment made for a Fe_3C monocrystal (that is, for annealed samples) [26]: $E_{\mathrm{MA}}^{\mathrm{exp}} = 6.97 \times 10^{5}\ \mathrm{J\,m^{-3}}$. The difference may be ascribed to the calculation inaccuracy or to a possible intermixture of carbon in the octahedral environment in the experiment.

For the case with carbon in the octahedral environment, $E_{\mathrm{MA}} < 10^{5}\ \mathrm{J\,m^{-3}}$, and this is clearly an order of magnitude lower than that calculated for the prismatic environment and, perhaps, does not essentially differ from $E_{\mathrm{MA}}^{\mathrm{exp}}$ of pure iron $6 \times 10^{4}\ \mathrm{J\,m^{-3}}$.

Using a simple model of interacting magnetic moments along the easy axis, one can find the domain-wall width $\delta = \pi l \sqrt{E_{\mathrm{exch}}/E_{\mathrm{MA}}}$ (see, for example, [15, 27]). Here $l = 0.26$ nm is the closest distance between the iron atoms, and E_{exch} is the exchange energy per volume. It is estimated from the temperature of the ferromagnet–paramagnet phase transition ($T_{\mathrm{C}} = 480$ K [26]): $E_{\mathrm{exch}} \approx k_{\mathrm{B}} T_{\mathrm{C}} n_{\mathrm{Fe}}/(Z V_{\mathrm{cell}}) = 5.49 \times 10^{7}\ \mathrm{J\,m^{-3}}$, where k_{B} is the Boltzmann constant, n_{Fe} is the number of iron atoms in the unit cell, $Z = 11$–12 is the number of nearest iron neighbours of Fe atoms. This leads to $\delta_{\mathrm{pris}} \approx 6.1$ nm. Such a domain wall should be effectively pinned to defects larger than 10 nm. Because in [14] the samples studied were in a nanocrystalline state with an average grain size of nanocrystals ranging from 10 to 60 nm (figure 3), it is natural to assume that they are the places of pinning of the domain walls. In the octahedral case, the domain-wall width is 4–5 times larger ($\delta_{\mathrm{oct}} \approx 25$–$30$ nm), and nanocrystals smaller than 30 nm are of no significance in the formation of the coercive force.

These considerations of the domain-wall width and the sizes of nanocrystals allow us to explain qualitatively the room-temperature behaviour of the coercive force as a function of the temperature of annealing of the plastically deformed cementite. Really, assuming that the initial samples are a mixture of the two phases (with prismatic and octahedral environments of carbon), we can assert that the amount of the metastable phase (with octahedral environment of carbon) decreases with annealing temperature. As a wide domain wall (in the octahedral case) has a number of pinning centres far less than the narrow one (the prismatic case), a decrease of the relative amount of the metastable phase should result in a drastic increase of the coercive force (figure 3).

It is again worth noting that if the plastically deformed samples in [14] consist only of a single phase with prismatic environment of carbon whose domain wall is narrow, annealing would only decrease the number of pinning centres, the domain-wall width remaining

constant. Then, the coercive force would decrease, which clearly contradicts the experiment. Apparently, this mechanism determines the behaviour of the coercive force during annealing at a temperature above 700 K (figure 3) because at this annealing temperature, as most experimenters believe [10, 13, 14], the samples have a sole, well-determined, structure with prismatic environment of carbon with maximum coercive force.

However, despite the large difference in E_{MA} between the prismatic and octahedral cases, the magnitudes of spin or orbital magnetic moment do not differ very much (see tables 3 and 4). The difference between the magnetic moments in prismatic and octahedral cementite are found to be numerically small, so the magnetic measurements are not expected to determine which carbon position is realized in samples.

The parameters of the hyperfine interaction are presented in tables 3 and 4. The isomer shift is obtained from the magnitude of the electron density at a point close to the Fe-nucleus centre. As there is no way to obtain the isomer shift unambiguously from calculations, we have conducted a calibrating calculation of the Fe_3Si alloy with the method described in section 2 and, in particular, with the same first radial-mesh point of the wave-function expansion in the MT sphere of Fe. Fe_3Si has two nonequivalent positions of iron atoms with different isomer shifts well-resolved experimentally; two experimental isomer shifts and the corresponding calculated electron densities gave us a desired functional dependence.

V_{zz} and V_{xx} are the maximum-in-magnitude and the minimum-in-magnitude components of the tensor of the electric field gradient (EFG). $\eta = (V_{xx} - V_{yy})/V_{zz}$. θ and ϕ are the polar and azimuthal angles of the hyperfine magnetic field H in the local coordinate system of the EFG. We have calculated the quadrupole splitting $\Delta = 0.5e^2Q|V_{zz}|(1 + 1/3\eta^2)^{1/2}$ ($eQ = 0.15 \times 10^{-28}$ m^2, Q is the nucleus quadrupole moment; see [28]). Measurement of the quadrupole splitting above the Curie temperature was performed in [29] for well-annealed samples, so the values obtained in [29] should be attributed to the ground state and can be compared to Δ calculated for the modification with the prismatic environment of carbon.

Table 3 shows the agreement between the experimental and calculated Δ for the prismatic case. The large quadrupole splitting as well as the differences in hyperfine parameters and angles (see tables 3 and 4) between the octahedral and prismatic cases allow us to hope that some difference in the form of the Mössbauer spectrum may be experimentally observed for these modifications of cementite.

When interpreting such Mössbauer experiments difficulties arise because both electric and magnetic interactions are present simultaneously (for example, see [30]). Indeed, the combined hyperfine interaction, and the angle between the hyperfine magnetic field and the electric field gradient, as well as the spatial averaging, essentially complicate the interpretation of a Mössbauer spectrum. Therefore, the analysis of Mössbauer spectra of cementite below the Curie temperature taking into account the present calculated parameters of the hyperfine interaction is of utmost interest.

4. Conclusions

Structural considerations of cementite show that carbon can occupy prismatic or octahedral pores in the iron sublattice. The present first-principles calculations confirm that the prismatic case possesses the lowest total energy and proves that the energy difference between the octahedral and prismatic modifications is smaller than the characteristic energy of plastic deformations during mechanical alloying. Thus, plastic deformation can strongly induce a rearrangement of the structure. The magneto-crystalline energy of cementite is much higher when the carbon atoms are in the prismatic pores in contrast with the case when the carbon atoms occupy the octahedral pores. The experimental room-temperature behaviour of the

coercive force of the plastically deformed samples as a function of annealing temperature can be explained by the rearrangement of the structure from the low-E_{MA} to the high-E_{MA} modification during annealing. Thus, the possibility of different carbon positions in cementite depending on the mechanical or thermal treatment is clearly confirmed by the experimental data (for example, [1]) and our first-principles calculations. The differences in the theoretical Mössbauer parameters between the prismatic and octahedral modifications of cementite looks promising for an experimental detection of the presence of carbon with octahedral environment in plastically deformed samples.

Acknowledgments

The authors are grateful to Professors E P Yelsukov and A I Ul'yanov for helpful discussions and for experimental data. This work was partially supported by INTAS (grant 03-51-4778), and RFBR (grant 07-03-96011).

References

[1] Elsukov E P, Dorofeev G A, Fomin V M, Konygin G N, Zagainov A V and Maratkanova A N 2002 *Phys. Met. Metallogr.* **94** 356
[2] Reed R C and Root J H 1998 *Scr. Mater.* **38** 95
[3] Koniger A, Hammerl C, Zeitler M and Rauschenbach B 1997 *Phys. Rev.* B **55** 8143
[4] Umemotoa M, Liu Z G, Masuyamab K and Tsuchiyaa K 2001 *Scr. Mater.* **45** 391–397
[5] Duman E, Acet M, Hulser T, Wassermann E F, Rellinghaus B, Itil J P and Munsch P 2004 *J. Appl. Phys.* **96** 5668
[6] Lin J-F, Struzhkin V V, Mao H, Hemley R J, Chow P, Hu M Y and Li J 2004 *Phys. Rev.* B **70** 212405
[7] Duman E, Acet M, Wassermann E F, Itie J P, Baudelet F, Mathon O and Pascarelli S 2005 *Phys. Rev. Lett.* **94** 075502
[8] Wood B J 1993 *Earth Planet. Sci. Lett.* **117** 593
[9] Vocadlo L, Brodholt J, Dobson D P, Knight K S, Marshall W G, Price G D and Wood I G 2002 *Earth Planet. Sci. Lett.* **203** 567
[10] Fasiska E J and Jeffrey G A 1965 *Acta Crystallogr.* **19** 463
[11] Schastlivtsev V M 2005 *Izv. Rus. Acad. Sci. Phys.* **69** 1292
[12] Schastlivtsev V M, Yakovleva I L, Mirzaev D A and Okishev K Yu 2003 *Phys. Met. Metallogr.* **96** 313
[13] Wood I G, Vocadlo L, Knight K S, Dobson D P, Marshall W G, Price G D and Brodholt J 2004 *J. Appl. Crystallogr.* **37** 82
[14] Yelsukov E P, Ul'yanov A I, Zagainov A V and Arsent'yeva N B 2003 *J. Magn. Magn. Mater.* **258/259** 513
[15] Herzer G 1997 Nanocrystalline soft magnetic alloys *Handbook of Magnetic Materials* vol 10, ed K H J Buschow (Amsterdam: Elsevier Science)
[16] Maratkanova A N, Ruts Y V, Surnin D V, Deev A N, Schastlivtsev V M, Yakovleva I L, Tabatchikova T I, Gusev S A and Salashchenko N N 2000 *Phys. Met. Metallogr.* **89** 604
[17] Elsukov E P, Fomin V M, Vytovtov D A, Dorofeev G A, Zagainov A V, Arsent'eva N B and Lomaeva S F 2005 *Phys. Met. Metallogr.* **100** 251
[18] Medvedeva I N, Kar'kina L E and Ivanovskii A L 2003 *Phys. Met. Metallogr.* **96** 452
[19] Haglund J, Grimvall G and Jarlborg T 1991 *Phys. Rev.* B **44** 2914
[20] Kokalj A 1999 *J. Mol. Graphics Modelling* **17** 176
[21] Blaha P, Schwarz K, Madsen G K H, Kvasnicka D and Luitz J 2001 *WIEN2k, An Augmented Plane Wave +Local Orbitals Program for Calculating Crystal Properties* Karlheinz Schwarz, Techn. Universitat Wien, Austria ISBN 3-9501031-1-2
[22] Perdew J P, Burke S and Ernzerhof M 1996 *Phys. Rev. Lett.* **77** 3865
[23] Madsen G K H, Blaha P, Schwarz K, Sjöstedt E and Nordström L 2001 *Phys. Rev.* B **64** 195134
[24] Cottenier S, Vries B De, Meersschaut J and Rots M 2002 *J. Phys.: Condens. Matter* **14** 3275–3283
[25] Yelsukov E P and Dorofeev G A 2004 *J. Mater. Sci.* **39** 5071
[26] Blum P and Pauthenet R 1953 *Compt. Rend.* **237** 1501
[27] Landau L D and Lifshitz E M 1935 *Sow. Phys.* **8** 157
[28] Martinez-Pinedo G, Schwerdtfeger P, Caurier E, Langanke K, Nazarewicz W and Sohnel T 2001 *Phys. Rev. Lett.* **87** 062701
[29] Ron M and Mathalone Z 1971 *Phys. Rev.* B **4** 774
[30] Blaes N, Fischer H and Gonser U 1985 *Nucl. Instrum. Methods Phys. Res.* B **9** 201